Biochemical and Biophysical Research Communications 586 (2022) 143–149

Contents lists available at ScienceDirect

Biochemical and Biophysical Research Communications

journal homepage: www.elsevier.com/locate/ybbrc

The RGD (Arg-Gly-Asp) is a potential cell-binding motif of UNC-52/PERLECAN

Zhongqiang Qiu, Aileen Park, Lianzijun Wang, Rachel Wilsey, Myeongwoo Lee*

Department of Biology, Baylor University, Waco, TX, 76798, USA

ARTICLE INFO

Article history:
Received 19 November 2021
Received in revised form
22 November 2021
Accepted 23 November 2021
Available online 24 November 2021

Keywords:
ECM
Nematode
Actin
Basement membrane
Muscle
Talin
Integrin

ABSTRACT

UNC-52/perlecan is a basement membrane (BM) proteoglycan playing an essential role in the muscle cell attachment of *C. elegans*. The UNC-52 protein contains two RGD (Arg-Gly-Asp) motifs in domains III and IV, a well-characterized tripeptide known for binding to mammalian β integrin. To investigate the role of the RGD motif in UNC-52/perlecan, we created two mutations in the ^{2021}RGD^{2023} motif: one mutation changed the RGD to an RGE, and the other deleted the RGD motif. The RGE^{2023} caused defective actin filaments and aberrant localization of PAT-3 β integrin and TLN-1/talin. Additionally, the in-frame deletion of RGD^{2023} resulted in a paralyzed and arrested at two-fold embryonic stages (Pat) phenotype, which is the identical phenotype of the *pat-3* β integrin null allele. These results indicate that RGD^{2023} is a potential ligand for cell binding and is essential for development and survival. Furthermore, our analysis reveals that the RGD of an invertebrate BM molecule is a potential cell-binding motif, suggesting that the function of the RGD motif is conserved among species.

1. Introduction

The extracellular matrix (ECM) and the basement membrane (BM) are protein-rich matrices deposited in the surroundings of tissue cells. The ECM is composed of essential biological molecules, such as glycoproteins and proteoglycans. The BM is a densely assembled ECM layer attached to the tissue borders. The ECM proteins bind to cell surface receptor integrins to regulate cell behaviors such as cell migration, adhesion, proliferation, and differentiation [1]. In particular, a distinctive motif in ECM proteins is recognized by the β integrin ligand-binding domain. Further studies have revealed that β integrin recognizes the tripeptide motif RGD (Arg-Gly-Asp) in the ECM proteins [2].

Perlecan, a heparan sulfate proteoglycan (HSPG), is a component of the ECM and the BM [3] and is involved in many biological functions, including growth factor binding, cell adhesion, cell growth, and tumor metastasis. Perlecan knock-out mice result in embryonic lethality due to abnormal ECM organization [4]. The RGD motif is incorporated into the laminin IVa domain (L4a) [5]. A synthetic RGD peptide blocks perlecan binding to β1 integrin expressing cells [6]. However, it is unknown whether this RGD directly interacts with β integrins *in vivo* model system [7]. UNC-52/perlecan is a *C. elegans* proteoglycan, a basement membrane component produced by muscles and hypodermis. UNC-52 is deposited on the exterior of muscle, pharynx, gonad, and intestine. It also plays an essential role in maintaining cell attachment, organ formation, and cell motility [8,9]. In their protein sequences, two RGD motifs are embedded in the laminin L4a domain of exon 7 (domain III) and on a C2 immunoglobulin-like (Ig-like) repeat of exon 19 (12th Ig-like repeats in domain IV) [10] (Fig. 1). Our previous analysis on a UNC-52 RGD motif revealed that the *unc-52(kq748),* RGE^{748}, and *unc-52(kq745),* RGD deletion (ΔRGD), displayed no prominent phenotype except for a mild motility defect [11].

Here, we report that ^{2021}RGD^{2023} of UNC-52/perlecan is essential for cell binding because 1) RGE^{2023} mutation caused severe Unc, 2) in-frame deletion of the RGD caused a paralyzed arrested at two-fold embryo stages (Pat) phenotype, and 3) RGE^{2023} mutation caused disrupted localization of PAT-3 β integrin and TLN-1/talin. Thus, our data suggest that the RGD^{2023} motif is a potential ligand for cell binding in *C. elegans*.

* Corresponding author.
E-mail address: Myeongwoo_Lee@baylor.edu (M. Lee).

https://doi.org/10.1016/j.bbrc.2021.11.083
0006-291X/

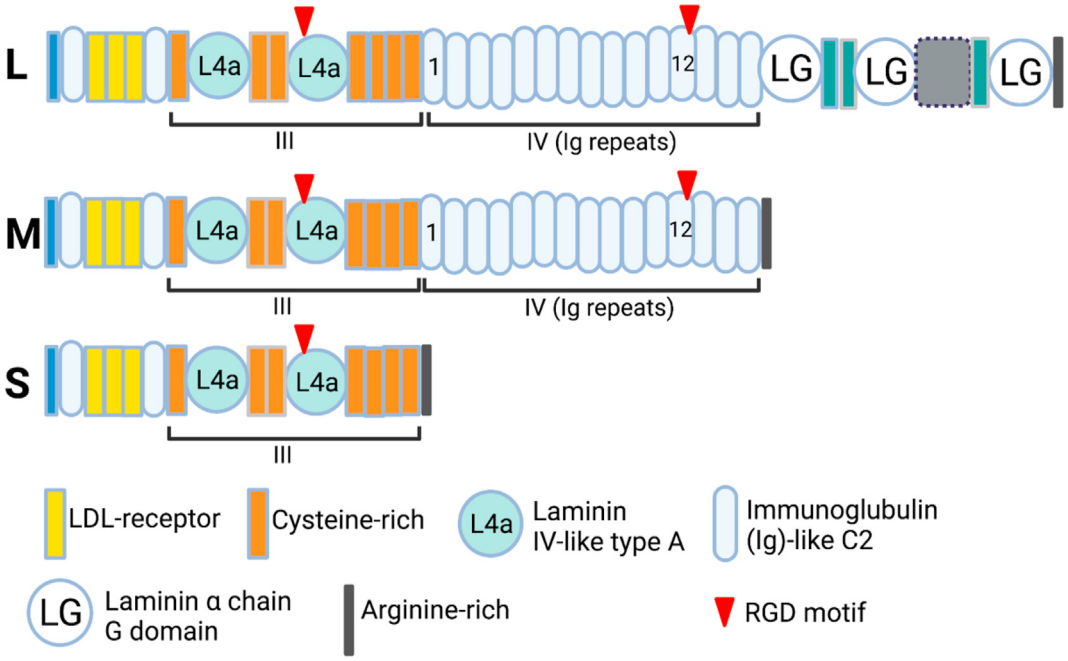

Fig. 1. Diagram of the UNC-52 protein [8]. UNC-52/perlecan is a secreted extracellular protein with five functional domains. Domains III and IV comprise multiple functional repeats or domains such as immunoglobulin-like (Ig-like) repeats, laminin IV-like type A (L4a) and laminin α chain globular domains (LG), and cysteine-rich repeats. The alternative-splicing of the unc-52 gene produces three protein isoforms, L, M, and S forms. * Red arrowheads indicate the location of the RGD748 and RGD2023 motifs. (For interpretation of the references to colour in this figure legend, the reader is referred to the Web version of this article.)

2. Materials and methods

2.1. Animals and culture

Table S2 shows the nematode animals used in this study. Some strains used were purchased from Caenorhabditis Genetics Center at the University of Minnesota, St. Paul, MN. All transgenic, mutant, and genome-edited lines were cultured on nematode growth medium (NGM) agar plates seeded with OP50 *E. coli* strain at room temperature.

2.2. CRISPR-Cas9 gene editing

CRISPR-Cas9 technology was used to create all *unc-52* mutants listed in Table S2. For the *unc-52*(RGE^{2023}) mutation, the DNA repair template (UNC52RGE2023), crRNA (UNC52RGD2023), tracrRNA (cat. #1072532), Cas9 nuclease (cat. #1081058), and a *dpy-10* crRNA co-CRISPR marker were mixed and micro-injected into wild-type N2 worms, which served as the parent (P0) generation. F1 worms that carried the mutation were then identified and isolated using the *dpy-10* marker [12,13] and underwent PCR genotyping using mutant-specific primers (UNC52RGE2023F and UNC52RGD2023SEQR) to screen for the RGE mutation. To identify the intended mutation from CRISPR animals, we performed single worm PCR. The F1 co-CRISPR Dpy progeny were isolated and submerged in 10 μl of Worm Lysis Buffer (1 mg/ml proteinase K in 1x NEB standard *Taq* polymerase buffer). The worms were frozen at −80 °C for 30 min, digested at 65 °C for 90 min (digestion), and inactivated at 95 °C for 15 min. The lysed reaction was used as a template in the following PCR reaction. The primers used in this study are listed in Table S3. The F2 generation then underwent PCR screening using both a mutant-specific primer (UNC52RGE2023F) and a wild-type specific primer (UNC52RGD2023WTF) to isolate homozygous mutants. These homozygous mutants were PCR amplified with the primer pair (UNC52RGD2023SEQF and UNC52RGD2023SEQR) flanking the mutation site. The *unc-52* RGE^{748} and ΔRGD mutations were generated by using the DNA repair template and the primers as indicated in our previous study [11]. The *kq2020* ΔRGD was also generated by using the single-stranded DNA repair template (UNC52RGD2023D). All oligos listed in Table S3 were designed at and purchased from IDT Inc., Coralville, IA. Finally, the RGE^{748} RGE^{2023} double RGE mutant was generated similarly. The UNC52RGD2023 crRNA was injected into RGD^{748} animals to generate the double RGE *unc-52* mutant. The genomic DNA of all edited lines was isolated and sequenced to verify mutations. All mutants were backcrossed to N2 at least two times to remove any background mutations. For each cross, F2 isolates were PCR verified.

2.3. Genetics and phenotype characterization

A double mutant was then created by crossing *unc-52* II mutant hermaphrodites with NK358 *pat-3::GFP* III males. Homozygous double mutants from the F2 generation were identified as green-fluorescent progeny and confirmed by PCR genotyping. Phenotypic assays were conducted on fifty young adult worms from both *unc-52* homozygous mutants and N2 wild-type worms. For thrashing assays, worms were placed in a 50 μl droplet of M9 buffer, and body bending was counted for 60 s after a 1-min acclimation period. The *kq2020*/+ was crossed to *mnC1[dpy-10(e128) unc-52(e444)]*/+ animals to generate a balanced strain, *kq2020/mnC1 [dpy-10(e128) unc-52(e444)]*.

2.4. Fluorescence microscopy and immunofluorescent staining

Fluorescence taining was performed by collecting mutants and fixing them with ice-cold methanol and acetone for 5 min. The rhodamine-phalloidin was used in 0.4 U/ml concentration, which is purchased from Sigma-Aldrich, St. Louis, MO. Images were captured using a Nikon Eclipse Ni–U epifluorescence or Olympus

FV-3000 confocal microscope and processed with NIS Elements (version 5.02). MH3 (1:200) monoclonal antibody was diluted with 1% goat serum in M9 buffer for immunofluorescence staining. Prepared primary antibodies covered fixed samples for 2–4 h at room temperature. After incubation, the sample was washed with M9 buffer three times. Goat anti-mouse IgG rhodamine-conjugated (Jackson Laboratory) was diluted 1:1000 in 1% goat serum solution, applied to the washed samples, and incubated overnight at 4 °C. After the treatment, the samples were rewashed and mounted with a coverslip for observation. The samples were examined on the Nikon Ni epifluorescence microscope. Images were processed with NIS elements software, as mentioned above.

2.5. Statistical analysis

In order to determine the statistical significance of differences between means, a one-way ANOVA test was used. Results from this statistical analysis are shown in Table S1, where p-values marked with asterisks (*) are statistically significant ($p < 0.05$).

3. Results and discussion

3.1. The unc-52 RGD mutations were generated for this study

In order to study the role of cell-binding motifs in UNC-52/perlecan, we generated mutations in a UNC-52 RGD motif, amino acid sequence ^{2021}RGD^{2023} (Fig. 1). For the RGD sequence, we generated an aspartic acid (D) to glutamate (E) mutation in the third amino acid position and the deletion of the motif, ΔRGD. The D to E mutation was introduced in the RGD motif to generate a mutation that disrupts the RGD motif but results in minimal disruption of the entire protein structure. For each allele, homozygote mutants were isolated. Each edited line was designated as alleles *kq2023* (RGE^{2023}), *kq748 kq2023* (RGE$^{748/2023}$, double RGE), or *kq2020* (ΔRGD^{2020}). In addition to ^{2021}RGD^{2023} mutations, we utilized *kq748* (RGE^{748}) and *kq745* (ΔRGD^{745}) alleles [11] for comparison studies as well as the CB444 *unc-52(e444)* mutant as a loss-of-function control. We then examined homozygote mutants for defective phenotypes in behavior, muscle filament, and gonad morphologies.

3.2. Initial phenotype analysis to identify the defects caused by unc-52 mutations

After isolating *unc-52* homozygotes, we performed a behavioral analysis to identify potential behavioral defects caused by the mutations. In *C. elegans*, the motility behavior of animals can be measured by counting the number of thrashes in an aqueous solution [14]. The *unc-52* mutant animals were placed in M9 buffer, and thrashing was measured for 60 s (Materials and Methods). Compared to the N2 wild-type, *unc-52(RGE^{2023})* displayed decreased motility in the thrashing assay (Table S1). While *unc-52(ΔRGD^{745})* animals showed motility (96.47 thrashes per min.) only slightly lower than the N2 wild-type animals (98.70 thrashes per min., $p = 0.9328$), *unc-52(RGE^{748})* animals displayed increased motility in comparison to N2 (107.16 thrashes per min., $p < 0.02356$) (Table S1). Our previous analysis characterized that the morphology of ΔRGD^{745} and RGE^{748} mutants were wild-type, showing few discernible differences [11].

The increased thrashing of RGE^{748} compared to RGE^{745} and N2 prompted us to create a double RGE mutant in the *unc-52* gene. The crRNA used to generate RGE^{2023} was microinjected into RGE^{748} animals, generating the homozygote RGE$^{748/2023}$ double mutant. The homozygous double RGE mutant was viable. However, the double RGE line showed lower motility (47.8 thrashes per min.) than the RGE^{2023} mutant (56.22 thrashes per min., $p = 0.004892$), suggesting that the RGE^{2023} and RGE^{748} mutations had a summative effect, resulting in a more severe behavioral phenotype when both present (Table S1).

3.3. The ΔRGD^{2020} is pat, paralyzed and arrested at the two-fold embryonic stage

Williams and Waterston (1994) identified the null allele of *the unc-52* gene [15]. The *unc-52(st549)* allele displays the Pat phenotype, similar to *pat-2* and *pat-3* integrin mutant phenotypes. The identical loss-of-function phenotype of the two genes, *unc-52* and *pat-3,* might indicate that these two genes are linked together. If there is a presumed direct or indirect interaction of two genes, the removal of either gene should result in the same phenotype [16]. The *st549* mutation, located in exon 7 of the gene, creates a premature termination codon [10] forty two amino acids downstream of RGD^{748}. According to the available splicing record of the gene, exon 7 is present in all isoforms of the UNC-52 protein, suggesting that the null mutation must have deleted the ^{2021}RGD^{2023} motif, a potential cell-binding motif to integrin.

To demonstrate the role of the RGD^{2023} motif, we created another CRISPR-edited line that deletes the ^{2021}RGD^{2023} motif. Similar to the method used to generate the RGE^{2023} allele, the *unc-52(kq2020,* ΔRGD^{2020}*)* was created (Materials and Methods) [17]. A heterozygous F1 animal was grown on an NGM agar plate, and hatched worms were monitored. The arrested F2 worms appeared to hatch but failed to grow more significantly than the two-fold embryo stage. A Nomarski image of a ΔRGD^{2020} worm revealed that the homozygote animals were arrested at an embryonic stage (Fig. S1). The arrested embryos appeared to have developed pharynx and intestine granules in the body cavity, suggesting that the arrested animals developed many different tissues. However, the outer surface was folded and showed protrusions over the surface. Hatched but arrested animals, homozygous ΔRGD^{2020}, were prodded with eyelash hair. We failed to observe any movement by gentle prodding, suggesting that the hatched worms were completely paralyzed.

3.4. The localization of actin, PAT-3 integrin, and its interacting molecules is disrupted in unc-52 mutants

The motility defect of RGE^{2023} led us to examine the actin cytoskeleton of the *unc-52* alleles. Compared to RGE^{748} and ΔRGD^{745}, the RGE^{2023} animals showed interrupted and clumped filaments (Fig. 2). Actin staining of UNC-52 RGE$^{748/2023}$ double mutants also showed disrupted filament patterns. We observed the head region of the mutants because *C. elegans* head muscles tend to keep the intact appearance of muscle filaments even in some severe Unc mutants. The *unc-52(RGE^{2023})* head showed a less organized head muscle (actin filaments) appearance (Fig. 2E and F).

Studies on PAT-3 β integrin revealed that it is localized to the dense bodies and M-lines of body wall muscle and the somatic gonad [18]. Lee et al. found that defects in *pat-3* integrin caused defective migration of hermaphrodite gonad leader cells, distal tip cells (DTC) [19]. Therefore, the DTC migration was examined under Nomarski microscopy. In many cases, the RGE$^{748/2023}$ double mutant showed that the worms have cell migration defects; usually, a DTC failed to stop when they were coming back to the center on the dorsal surface, often passing the body center (above the vulva) or showing wavy patterns (Fig. S1).

Greg Mullen et al. described that loss-of-function *unc-52* mutations cause defective *pat-3* integrin localization in embryos [20]. Therefore, NK358 PAT-3:GFP [21] was crossed to *unc-52* mutants. The PAT-3:GFP in the body wall muscle of *unc-52* mutants also

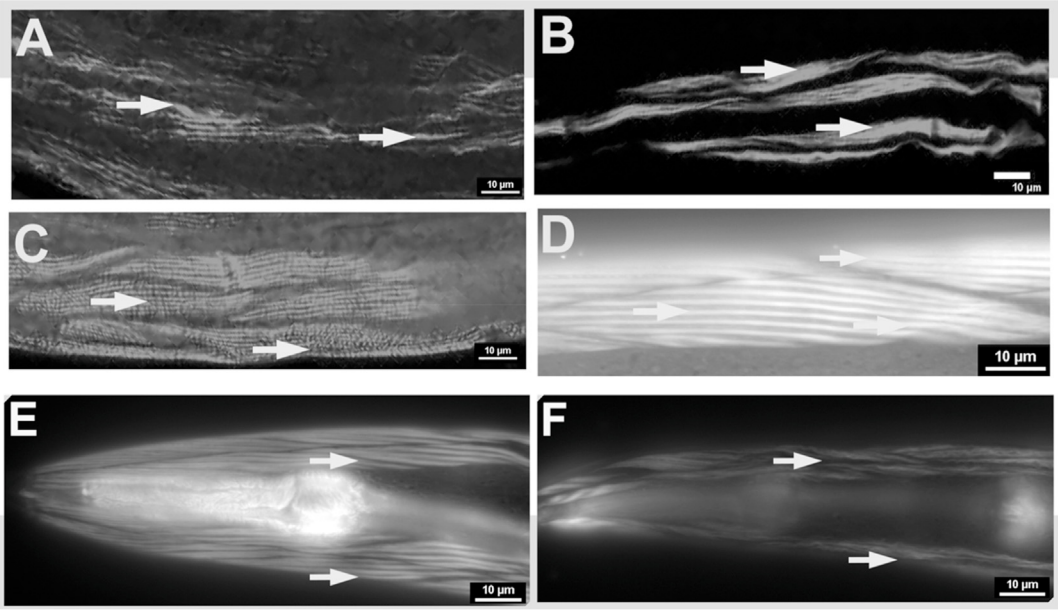

Fig. 2. The unc-52 mutant animals were stained with rhodamine-phalloidin. Panel A. Phalloidin staining of an unc-52(RGE748/2023) double RGE animal; panel B. unc-52(RGE2023); panel C. unc-52(RGE748); panel D. N2. Panel E. Phalloidin staining of N2 animal. The anterior end region is shown here. Panel F. Phalloidin staining of unc-52(RGE2023) animal head is also shown here. Arrows indicate actin filaments.

showed defects in localization (Fig. 3). The GFP of the $RGE^{748/2023}$ double appeared patchy and failed to localize to regular dense bodies and M-line patterns (Fig. 3A). The PAT-3:GFP of RGE^{2023} showed similarities to $RGE^{748/2023}$ double mutant (Fig. 3C), while RGE^{748} showed typical dense bodies and M-line pattern, dotted lines along the line of muscle filaments, showing the same pattern as NK358 *pat-3*:GFP (Fig. 3E). The PAT-3:GFP in *unc-52(e444)* (Fig. 3G), a loss-of-function control, was similar to panels A and C, suggesting that the defective localization of *pat-3* comes from the *unc-52* mutation.

TLN-1/talin is a linker protein that connects integrin cytoplasmic tails to the actin cytoskeleton [22]. The actin and integrin defects in the RGE^{2023} animal prompted us to investigate the localization of the downstream linker protein in *unc-52* mutants. Our data suggested that TLN-1 localization was abnormal since it failed to show regular dense bodies and M-lines. Instead, RGE^{2023} and $RGE^{748/2023}$ double mutants showed patchy and aggregated patterns in the shape of muscle cells; they showed discontinuous and lumpy filaments localized in the mutant muscles (Fig. 3B and D). In summary, the distribution of PAT-3 β integrin and TLN-1/talin appeared disorganized in the *unc-52* muscle cells. Furthermore, we also described that actin filaments are disorganized in *unc-52(*RGE^{2023}*)* mutants. Thus, our data suggest that the intact RGD^{2023} motif of UNC-52 is required for the proper localization of integrin and muscle filament organization.

3.5. Distribution of UNC-52/perlecan in the unc-52 mutants

Our analysis indicated that mutations in the RGE^{2023} motif cause severe phenotypes. In particular, the *unc-52(kq2020,* ΔRGD^{2020}) allele displayed the Pat phenotype, which is deletes three amino acids in-frame. Mullen et al. (1999) described nine in-frame deletions in exons 15 to 18, which showed no apparent defects [8,10]. The severe phenotypes in *unc-52(*ΔRGD^{2020}*)* and *unc-52(*RGE^{2023}*)* mutants prompted us to examine the localization pattern of UNC-52 protein in the mutant background. The ΔRGD^{2020} embryos and RGE^{2023} worms were fixed and stained with MH3 monoclonal antibody against UNC-52 [23] to measure the distribution of the mutant proteins.

The MH3 immunofluorescence was deposited over the surface of muscle cells. In N2 animals, the UNC-52 protein appeared between the hypodermis and muscle cells. Dense bodies and M-lines were displayed under the surface in a deeper focal plane (Fig. 4). The primary layer of the fluorescence was on the surface of body wall muscles. More fluorescence was evident on the muscle cell boundary lines. In body wall muscles, cell-to-cell boundaries include a distinct feature in which ECM molecules formed deeper cell-matrix structures between muscle cells [24]. In Fig. 4, both N2 and mutant muscles showed more intense staining on the muscle cell boundaries. The RGE^{2023} animals showed a typical MH3 staining pattern over the withered and clumped muscle appearance (Fig. 4B and E). We also stained ΔRGD^{2020} arrested embryos, which displayed an accumulation of the UNC-52 protein along the embryo body wall. In addition, detachment of muscles from the body wall was apparent (Fig. 4D). MH3 staining demonstrated that *unc-52(*RGE^{2023}*)* and *unc-52(*ΔRGD^{2020}*)* mutants express UNC-52/perlecan proteins and confirmed that the mutations did not eliminate the UNC-52 protein.

In summary, we created two mutations in RGD^{2023}, one replacing D for E and another deleting the RGD motif. The RGE^{2023} allele displays an uncoordinated movement (Unc) phenotype, and ΔRGD^{2020} appears Pat, an embryonic lethality, suggesting the essential nature of RGD^{2023}. Also, $RGE^{748/2023}$ double mutants showed additive effects on behavioral defects. To our surprise, the ΔRGD^{2020} was arrested at a two-fold embryo, even though the mutant protein is expressed.

Since discovering the RGD motif, researchers have focused on the binding ability of purified RGD proteins in cell culture systems. While the RGD motif became recognized as a binding motif for β integrin receptors, a genetic approach to deleting or modifying the RGD in ECM has not been extensively attempted. Although there is a report about the RGD containing domain deletion in *the Drosophila tiggrin* gene [25], few attempts in the invertebrate model system have been carried out to precisely characterize the RGD

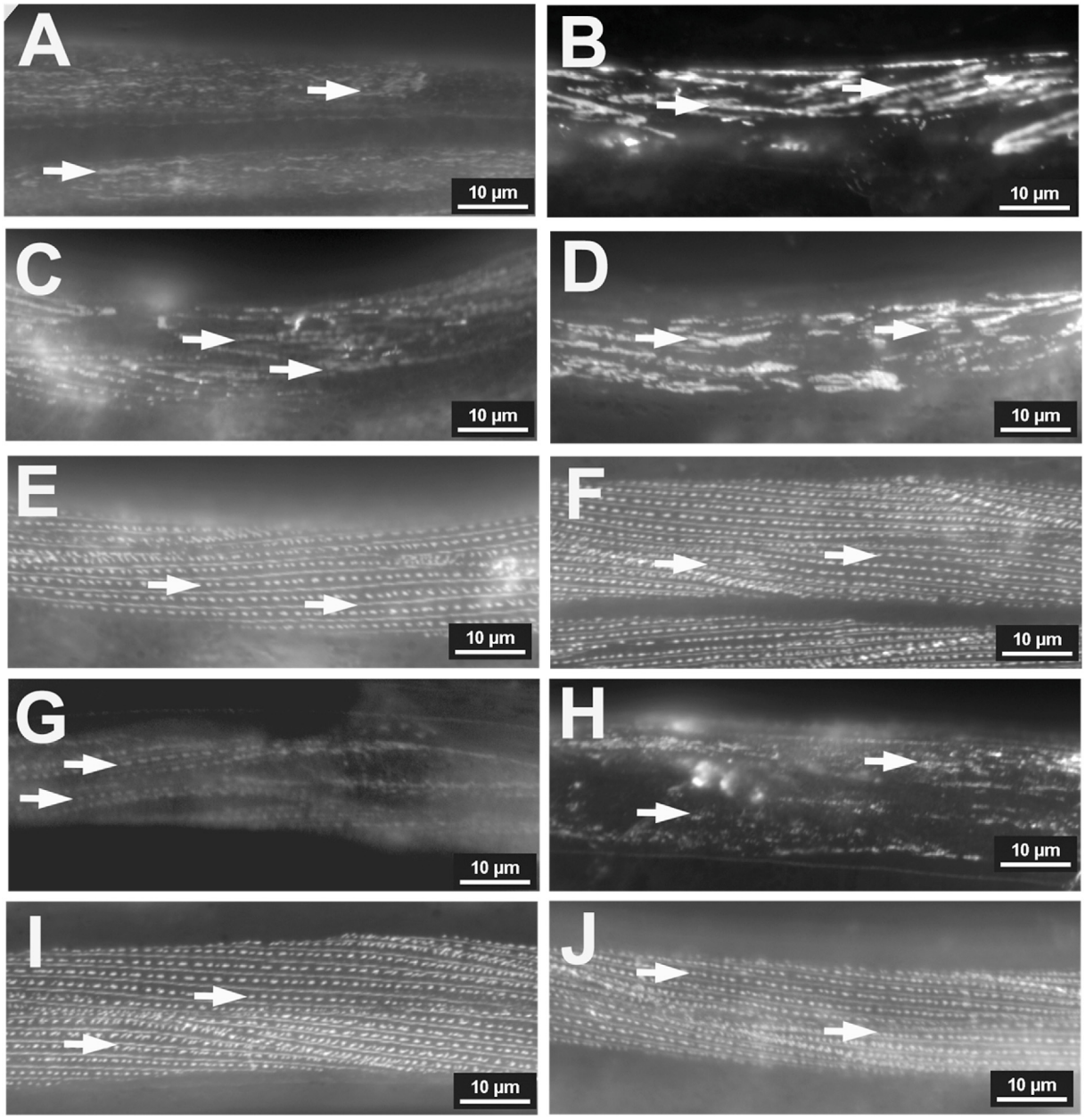

Fig. 3. Localization of PAT-3 β integrin and TLN-1/talin in unc-52 mutants. Panels A and B. unc-52(RGE748/2023) animals; panels C and D. unc-52(RGE2023); panels E and F. unc-52(RGE748); panels G and H. unc-52(e444) as a control mutant; panels I and J. N2 animals, as wild-type control. Panels A, C, E, G, and I are pat-3:GFP in mutants and control background. Panels B, D, F, H, and J are TLN-1/talin:GFP in mutants and control background. Arrows indicate dense bodies in muscle cells, dotted lines along the length of muscle cells. Panels H and J are 60X magnification.

motif in their ECM proteins.

Our research takes an *in vivo* approach to measuring the function of the RGD motif at an organism level. Highlights of our findings are that UNC-52 RGD^{2023} appears essential to the animal function and that the deletion (ΔRGD) showed a Pat phenotype that is shared by mutations in other ECM genes such as collagen IV [26], integrins [27], and *unc-97*/PINCH [28]. This RGD motif is located in exon 19, included in M and L, but not in S, UNC-52 proteins. This result suggests that the M and L forms of UNC-52/perlecan use RGD^{2023} for cell binding. RGD^{748} fails to display severe defects, suggesting that RGD^{748} may have a different role in addition to acting as a cell-binding motif, even though RGD^{748} is incorporated in all UNC-52 protein isoforms. The importance of our study is that ΔRGD^{2020}, the deletion of RGD^{2023}, caused a Pat phenotype while still expressing the mutant UNC-52 protein. The mutant embryo is arrested at the two-fold stage because that is the developmental period in which muscle starts to elongate and forms attachments to the basement membrane (BM) using αPAT-2/βPAT-3 integrin [29]. Taken together, it is apparent that RGD^{2023} is indispensable for muscle development. Therefore, the removal of RGD^{2023} gives the same result as the null phenotype of *unc-52, pat-2, and pat-3* [15].

Our results from studies of *unc-52* provide us with valuable information to understand the potential role of the RGD motif. It shows that RGD motifs in UNC-52 RGD^{2023} work similarly to the mouse or human RGD motif in fibronectin [30], strongly suggesting that it binds to integrin, a cell surface receptor for ECM. Nevertheless, the biochemical interaction between UNC-52/perlecan and PAT-3/β integrin must be addressed in a future study. Furthermore,

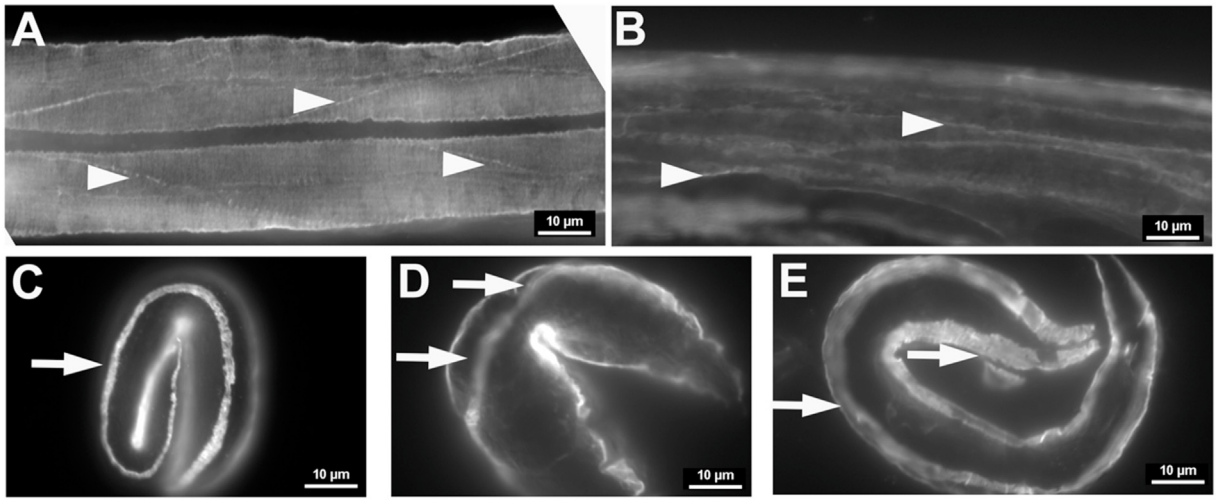

Fig. 4. The N2 and unc-52 mutants were stained with MH3 monoclonal antibodies. The wild-type N2 and mutant animals were stained with MH3 as a primary antibody and Cy3-conjugated anti-mouse IgG as secondary antibodies (Materials and Methods). Panel A. N2 animal showing UNC-52 distribution over muscle surface. Arrowheads indicate the muscle cell boundaries; panel B. unc-52(RGE2023) shows defective UNC-52 distribution. Arrowheads indicate muscle cell boundaries; panel C. N2 embryo, an arrow points elongating musculature; panel D. unc-52(ΔRGD2020) arrested embryo was stained with MH3. Arrows are pointing detached body wall muscle; panel E. unc-52(RGE2023). The RGE2023 mutation develops muscles in the embryo.

our study brings a new approach to studying cell-binding motifs using an *in vivo* system; deletion or mutation in RGD or other cell-binding motifs will provide new findings related to ECM-cell interaction at the whole organism level.

Declaration of competing interest

Authors declare no conflict of interest to the project described in the manuscript above.

Data availability

No data was used for the research described in the article.

Acknowledgments

Authors thank Baylor University for funding and Drs. Jae Hyoung Cho and Adam Wright at the WORMBASE for identifying RGD proteins in *C. elegans* genome. Siena Bertoluzzi, Olineece Croomes, Emily Johnson, Meagan Marquez, and Morenike Tajudeen were the BIO4108 students who studied *unc-52(kq2023)* for Summer 2019. We also thank Dr. Daniel Dickinson at the University of Texas for his advice and encouragement, which led us to adopt the CRISPR-Cas9 system.

Appendix A. Supplementary data

Supplementary data to this article can be found online at https://doi.org/10.1016/j.bbrc.2021.11.083.

References

[1] R.O. Hynes, The evolution of metazoan extracellular matrix, J. Cell Biol. 196 (2012) 671–679, https://doi.org/10.1083/jcb.201109041.
[2] E. Ruoslahti, RGD and other recognition sequences for integrins, Annu. Rev. Cell Dev. Biol. 12 (1996) 697–715, https://doi.org/10.1146/annurev.cellbio.12.1.697.
[3] R.V. Iozzo, I.R. Cohen, S. Grassel, A.D. Murdoch, The biology of perlecan: the multifaceted heparan sulphate proteoglycan of basement membranes and pericellular matrices, Biochem. J. 302 (Pt 3) (1994) 625–639, https://doi.org/10.1042/bj3020625.
[4] M. Costell, E. Gustafsson, A. Aszodi, M. Morgelin, W. Bloch, E. Hunziker, K. Addicks, R. Timpl, R. Fassler, Perlecan maintains the integrity of cartilage and some basement membranes, J. Cell Biol. 147 (1999) 1109–1122, https://doi.org/10.1083/jcb.147.5.1109.
[5] H. Colognato, P.D. Yurchenco, Form and function: the laminin family of heterotrimers, Dev. Dynam. 218 (2000) 213–234, https://doi.org/10.1002/(SICI)1097-0177(200006)218:2<213::AID-DVDY1>3.0.CO;2-R.
[6] K. Hayashi, J.A. Madri, P.D. Yurchenco, Endothelial cells interact with the core protein of basement membrane perlecan through beta 1 and beta 3 integrins: an adhesion modulated by glycosaminoglycan, J. Cell Biol. 119 (1992) 945–959, https://doi.org/10.1083/jcb.119.4.945.
[7] R.V. Iozzo, Perlecan: a gem of a proteoglycan, Matrix Biol. 14 (1994) 203–208.
[8] G.P. Mullen, T.M. Rogalski, J.A. Bush, P.R. Gorji, D.G. Moerman, Complex patterns of alternative splicing mediate the spatial and temporal distribution of perlecan/UNC-52 in Caenorhabditis elegans, Mol. Biol. Cell 10 (1999) 3205–3221, https://doi.org/10.1091/mbc.10.10.3205.
[9] T.M. Rogalski, G.P. Mullen, J.A. Bush, E.J. Gilchrist, D.G. Moerman, UNC-52/perlecan isoform diversity and function in Caenorhabditis elegans, Biochem. Soc. Trans. 29 (2001) 171–176, https://doi.org/10.1042/0300-5127:0290171.
[10] T.M. Rogalski, E.J. Gilchrist, G.P. Mullen, D.G. Moerman, Mutations in the unc-52 gene responsible for body wall muscle defects in adult Caenorhabditis elegans are located in alternatively spliced exons, Genetics 139 (1995) 159–169.
[11] R. Wilsey, S. Hodge, K. Kenney, J. Wahl, R. Jaffery, A. Brau, Z. Qiu, M. Lee, Two alleles of unc-52 locus disrupting potential cell-binding motif of UNC-52, MicroPubl Biol (2020) 2020, https://doi.org/10.17912/micropub.biology.000250.
[12] A. Paix, A. Folkmann, D. Rasoloson, G. Seydoux, High efficiency, homology-directed genome editing in Caenorhabditis elegans using CRISPR-Cas9 Ribonucleoprotein Complexes, Genetics 201 (2015) 47–54, https://doi.org/10.1534/genetics.115.179382.
[13] J.A. Arribere, R.T. Bell, B.X. Fu, K.L. Artiles, P.S. Hartman, A.Z. Fire, Efficient marker-free recovery of custom genetic modifications with CRISPR/Cas9 in Caenorhabditis elegans, Genetics 198 (2014) 837–846, https://doi.org/10.1534/genetics.114.169730.
[14] M. Koopman, Q. Peter, R.I. Seinstra, M. Perni, M. Vendruscolo, C.M. Dobson, T.P.J. Knowles, E.A.A. Nollen, Assessing motor-related phenotypes of Caenorhabditis elegans with the wide field-of-view nematode tracking platform, Nat. Protoc. 15 (2020) 2071–2106, https://doi.org/10.1038/s41596-020-0321-9.
[15] B.D. Williams, R.H. Waterston, Genes critical for muscle development and function in *Caenorhabditis elegans* identified through lethal mutations, JCB (J. Cell Biol.) 124 (1994) 475–490.
[16] J. Hodgkin, Genetic Suppression, WormBook, 2005, pp. 1–13, https://doi.org/10.1895/wormbook.1.59.1.
[17] D.J. Dickinson, B. Goldstein, CRISPR-based methods for Caenorhabditis elegans genome engineering, Genetics 202 (2016) 885–901, https://doi.org/10.1534/genetics.115.182162.
[18] S.N. Gettner, Isolation and Functional Analysis of *Caenorhabditis elegans* Integrin Bpat-3, University of California, San Francisco, CA, 1994.
[19] M. Lee, E.J. Cram, B. Shen, J.E. Schwarzbauer, Roles for beta(pat-3) integrins in development and function of Caenorhabditis elegans muscles and gonads, J. Biol. Chem. 276 (2001) 36404–36410, https://doi.org/10.1074/

jbc.M105795200, pii.
[20] G.P. Mullen, Localization and Function of UNC-52/Perlecan Isoforms in the Nematode Caenorhabditis elegans, Genetics, The Univeristy of British Columbia, Vancouver, Canada, 1998, p. 166.
[21] E.J. Hagedorn, H. Yashiro, J.W. Ziel, S. Ihara, Z. Wang, D.R. Sherwood, Integrin acts upstream of netrin signaling to regulate formation of the anchor cell's invasive membrane in C. elegans, Dev. Cell 17 (2009) 187–198, https://doi.org/10.1016/j.devcel.2009.06.006.
[22] E.J. Cram, S.G. Clark, J.E. Schwarzbauer, Talin loss-of-function uncovers roles in cell contractility and migration in C. elegans, J. Cell Sci. 116 (2003) 3871–3878, https://doi.org/10.1242/jcs.00705 [pii].
[23] G.R. Francis, R.H. Waterston, Muscle organization in *Caenorhabditis elegans*: localization of proteins implicated in thin filament attachment and I-band organization, JCB (J. Cell Biol.) 101 (1985) 1532–1549.
[24] H. Qadota, Y. Matsunaga, K.C.Q. Nguyen, A. Mattheyses, D.H. Hall, G.M. Benian, High-resolution imaging of muscle attachment structures in Caenorhabditis elegans, Cytoskeleton (Hoboken) 74 (2017) 426–442, https://doi.org/10.1002/cm.21410.
[25] T.A. Bunch, M.W. Graner, L.I. Fessler, J.H. Fessler, K.D. Schneider, A. Kerschen, L.P. Choy, B.W. Burgess, D.L. Brower, The PS2 integrin ligand tiggrin is required for proper muscle function in Drosophila, Development 125 (1998) 1679–1689.
[26] X. Guo, J.J. Johnson, J.M. Kramer, Embryonic lethality caused by mutations in basement membrane collagen of *C. elegans*, Nature 349 (1991) 707–709.
[27] S.N. Gettner, C. Kenyon, L.F. Reichardt, Characterization of bpat-3 heterodimers, a family of essential integrin receptors in *C. elegans*, JCB (J. Cell Biol.) 129 (1995) 1127–1141.
[28] O. Hobert, D.G. Moerman, K.A. Clark, M.C. Beckerle, G. Ruvkun, A conserved LIM protein that affects muscular adherens junction integrity and mechanosensory function in Caenorhabditis elegans, J. Cell Biol. 144 (1999) 45–57.
[29] D.G. Moerman, B.D. Williams, Sarcomere assembly in C. elegans muscle, WormBook (2006) 1–16.
[30] S. Takahashi, M. Leiss, M. Moser, T. Ohashi, T. Kitao, D. Heckmann, A. Pfeifer, H. Kessler, J. Takagi, H.P. Erickson, R. Fassler, The RGD motif in fibronectin is essential for development but dispensable for fibril assembly, J. Cell Biol. 178 (2007) 167–178, https://doi.org/10.1083/jcb.200703021.